Energetically Optimal Trajectory for a Redundant Planar Robot by Means of a Nested Loop Algorithm

Harold Potter, John Kern*, Guillermo Gonzalez, Claudio Urrea
Electrical Engineering Department, Faculty of Engineering,
University of Santiago of Chile (USACH),
Av. Ecuador 3519, Estacion Central, Santiago 9170124, Chile
john.kern@usach.cl

***Abstract*—This work presents an optimal point-to-point trajectory planning method based on fourth degree polynomials to reduce the energy consumption of a redundant planar robot in the XY plane. The contribution of this study focuses on the development of a two-level nested optimization algorithm, which manages to optimize three elements: the Optimal Weighting Vector that establishes the influence of each joint on the total energy consumption of the robotic equipment; the optimal start and finish configurations of the trajectory; and the vector corresponding to the fifth coefficient of the trajectory generator polynomial. The tests are carried out with different optimization techniques and objective functions related to energy consumption to determine their best combination and achieve the minimum possible computation time and energy savings, according to the test conditions used. Furthermore, the energetic performance of the redundant manipulator is compared with its non-redundant version, limiting its operation to only two degrees of freedom in all its variants.**

***Index Terms*—Redundant robot; Manipulator dynamics; Trajectory optimization; Software algorithms.**

I. INTRODUCTION

The last few years have been characterized by an increasingly demanding context for the productive sector, where rising energy prices and progressive social awareness of the care of the environment have established the scientific world's need to look for new solutions, with the aim of reducing energy consumption in production processes, where industrial robots play a very important role in automation technologies, with a market penetration that shows few signs of slowing. According to Carabin, Wehrle, and Vidoni [1], within the classification related to saving and optimizing energy consumption of Robotic Equipment (RE), there are two main families that stand out: software enhancement and hardware enhancement.

Stringent new requirements are ever more present in the industrial and productive sector. Pressures on productivity and company image have arisen in quite distinct ambits: social and environmental responsibility on one hand, and rising energy and raw material costs on the other. Both ambits require new scientific approaches. The impact on energy consumption of industrial robotic solutions in industrial automation is firmly established. The authors in [1] have shown that two outstanding areas of optimization related to improved Robotic Energy consumption are software enhancement and hardware enhancement.

The class of software improvement is mainly related to the optimization of RE trajectories. This seeks to minimize elements such as trajectory time, jerks, instabilities, and energy consumption in mechatronic and robotic systems. Hardware improvements include the replacement or addition of energetically efficient components through optimal system design.

In the process of planning optimal energy trajectories, many optimization techniques have been implemented on industrial manipulators with different Degrees of Freedom (DoF), as well as on mobile robots and other similar devices. Promising results have been obtained at the simulation level and in real implementations. This is the case of the technique of the subspace trust method [2], Euler/Runge Kutta with multiple method shooting [3], dynamic programming with Dubins routes [4], dynamic programming "Mixed Integer Nonlinear Programming" [5], Interior Point Optimizer (IP) [6], evolutionary model and swarm intelligence [7], differential evolution [8], gradient-based algorithm [9], dynamic programming [10], Kalman heuristic algorithm [11], Genetic Algorithm (GA) [12], metaheuristic algorithm type vector evaluated particle swarm optimization [13], sequential quadratic programming [14], Hessian and GA matrix [15], Pontryagin's minimum algorithm [16], and optimization of multiple immune targets of restrictions [17]. Finally, in [18], a trajectory planning method is developed based on a surrogate or substitute model for an unmanned electric excavator.

Similarly, to determine the energy used by the robotic manipulator, using an objective function, it is possible to consider different variables obtained from the RE operation

Manuscript received 30 December, 2021; accepted 25 February, 2022.
This work has been supported by Agencia Nacional de Investigación y Desarrollo ANID, Chile, through IDeA I + D ID21I10087 project and by Vicerrectoría de Investigación, Desarrollo e Innovación of the University of Santiago of Chile, Chile.

such as total work [13], some squared torque variants [3], [14], [19]; squared current [12], actuator motor power [5], [11], [15], [16]; squared acceleration [4], [17], [20]; potential and kinetic energy [8], mean square torque [9], [21] and mechanical power [9]. In addition, the authors consider the use of a weight vector that penalizes the influence of each joint in the optimization task, such as Zhao, Lin, and Tomizuka [22] and Wigstrom, Lennartson, Vergnano, and Breitholtz [5]. The authors use only fixed weight factors proportional to the transmission ratio of each actuator.

Regarding the functions used as a basis in the optimization process trajectory, a Spline function is often used in [6], [9], [14], [17], and [19]. In [13] and [15], a cycloidal path and an S-curve profile are used, respectively. In [12], a polynomial formulation of the 3rd and 4th degree is used. Finally, models such as the Rubins route and predesigned models are found to be advantageous in [4] and [11], respectively.

The importance of smoothness in the trajectory design of robot manipulators is a factor that produces, on the one hand, better movements according to specific tasks (e.g., pick and place, welding, etc.) and, on the other hand, more efficient trajectories in relation to energy consumption, which contributes to the autonomy of a robot [23]. Smooth trajectories can be achieved by optimizing the time derivative of the acceleration in a robot. In the same effort, the authors in [24] seek this goal, together with a reduction in the execution time of the trajectory using an improved GA algorithm in a 6 DoF manipulator. In the same way, in [25], employing an interior point solver and Legendre Polynomials, a solution for a manipulator with 6 degrees of freedom is developed. In optimizing execution time and smoothness, Zhang, Zhang, and Zou in [26] propose a novel algorithm to eliminate residual vibration and achieve smooth motion in a 6 DoF robot. Vysocký *et al.* in [27] reduces energy use in point-to-point paths together with ensuring smooth trajectories by using an optimization algorithm and Bezier curves as trajectory generator to achieve a natural smoothing mechanism. Furthermore, in planning smooth trajectories, the authors in [28] optimize the movements on a "Stewart" type rehabilitation platform 6 DoF parallel robot by sequential quadratic programming and cubic splines. In the planning trajectories research with multi-objective optimization, energy efficiency can be accompanied with many other combinations such as in [29], where a solution to solve the problem of optimal velocity, energy, and smoothness in a 7 DoF manipulator is proposed by means of a multi-objective PSO (particle swarm optimization) with 5th order cosine polynomial. Liu, Qiu, Zeng, Li, and Xie [30] have developed for a collaborative welding robot arrangement, an algorithm that optimizes both energy and time trajectory using PSO and B splines. Stuhlenmiller, Clever, Rinderknecht, Lutter, and Peters [31] propose a novel planning trajectory algorithm that aims to optimize the energy consumption and expected service life of a 7 DoF manipulator using interior point solver with 5th order polynomials. An additional consideration occurs in autonomous tasks such as fruit picking, where dependance on energy efficient planning and control algorithms ensure the longest working time. The works in [32] and [33] focus on this requirement where they develop trajectory planning systems based on multi-objective PSO and the heuristic method of shortcuts with third degree polynomial functions, respectively. Additionally, in tasks such as harvesting, the techniques of object avoidance are characterized by a short calculation time to plan an optimal trajectory. This requires that this variable be considered when designing the planning algorithm. In this way, together with the works cited above, the authors in [34] developed an energy optimization trajectory planning method for a 3 DoF manipulator using the kinetic energy integral in a limited subset of future end-effector path points. This approach achieved a computational time of less than a second.

On the other hand, frictional force has a significant effect on the actual performance of robotic systems. In recent years, work has been done on various models of friction and the identification of its parameters. Considering friction in an energy optimization model implies a significant contribution to real-world results. Therefore, Cezner [6], Hansen, Öltjen, Meike, and Ortmaier [9], and Pellegrinelli, Borgia, Pedrocchi, Villagrossi, Bianchi, and Tosatti [10] consider within their work the Coulomb-Viscous Frictions model. In another approach, Wigstrom, Lennartson, Vergnano, and Breitholtz [5] use the viscous friction model. Another, more complex, friction model (Stribeck) uses a first-order nonlinear differential equation, mentioned by Baressi Šegota, Anđelić, Lorencin, Saga, and Car in [19]. This is not implemented in this work. Finally, the works in [3], [13], [17], and [35] do not consider this resistance variable within the optimization model. Exploiting kinematics redundancy, as a tool to improve energy performance in RE tasks, is used in a number of cases, such as in [36], where a 4 DoF cell - robotic arrangement composed of a 3 DoF type Selective Compliant Articulated Robot Arm (SCARA) coupled to a 1 DoF linear unit - is used for a pick-and-place task. The numerical results achieved show an energy economy of around 65 % and a faster execution time compared to a non-redundant configuration. On the other hand, in [37], optimal path planning is presented for a 3 DoF redundant planar manipulator for point-to-point and continuous tasks; here, the minimization of energy consumption is achieved by considering restrictions in the kinematic and dynamics of the RE. Finally, in [38], the energy efficiency problem is presented for the case of a forestry loader, corresponding to a hydraulic 4 DoF kinematically redundant manipulator. In this case, the movement of the redundant extension cylinder was optimized; in front of three testing trajectories, verified values between 15 % and 30 % of efficiency are obtained, compared to alternative optimization methods.

The present work shows an approach focused on minimization, by means of software techniques, of the energy consumption of the rotational component of a 3 DoF redundant planar robot [39], in point-to-point trajectories, such as pick-and-place tasks present in industrial equipment. The contribution of this study focuses on the development of an algorithm of nested optimization of two loops, which

manages to relate the three following variables:

– The Optimal Weighting Vector (OWV) establishes the influence of each joint on the total energy consumption of robotic equipment;

– The optimal position of the joints, initial and final, contained in the Register of Joint Combinations (RJC);

– The optimal coefficient of the polynomial of the path generator.

As the basis of the calculation for the test trajectories, a fourth-order polynomial is used; furthermore, the main loop of the proposed algorithm is tested with the Genetic Algorithm (GA) and Surrogate Algorithm (SG) optimization techniques, both capable of solving the optimization problem of mixed integers. It is also used in the inner loop of the algorithm an Interior Point optimization algorithm (IP), which calculates the energetically optimum trajectory considering both the dynamics of the RE as well as the candidate values of the OWV and the RJC. Similarly, experiments were carried out with three different energy consumption analysis methods for the objective function, such as total work, mean square torque, and mechanical energy; all with the aim of determining the best combination of these techniques and methods to achieve the greatest computational economy and possible energy savings, according to the test conditions presented here. On the other hand, the optimized energy performance of the redundant manipulator is compared with the performance of its non-redundant versions. For this, its operation is limited to only two DoF in three possible variants, leaving a joint at 0 radians for each case.

II. PROBLEM STATEMENT

The present study focuses on minimizing the energy consumption of a manipulator robot during a certain point-to-point trajectory by means of software techniques, considering within the optimization algorithm a weighting factor related to the influence of each joint in the total energy consumption, and, at the same time, taking advantage of the best selection of initial and final joint configuration of a certain trajectory. In this way, the problem consists of finding a point-to-point, energy-efficient trajectory for a 3 DoF planar robotic manipulator in off-line mode, corresponding to the rotational component of a redundant robotic manipulator, and, at the same time, seeking the best possible economy of calculation. Also, given the kinematics-based approach presented in this work, it is proposed to verify the performance of this approach, in relation to that proposed in [39].

It is also known that kinematic redundancy can provide a RE with manipulative skill and versatility in its movement (the possibility of avoiding obstacles in the workplace, increased work area, joint collaboration, etc.). Finally, it is proposed to verify energy efficiency, produced by adding a degree of redundancy in a task developed in the XY plane by a 2 DoF RE.

A. Workspace and Kinematic Redundancy

The workspace described by an RE encompasses all the possible robot movements. It is characterized by its geometry and the mechanical limits of the joints and can be obtained by means of the position component ($\boldsymbol{p_e}$) [40] from the direct kinematic equation in terms of expression (1)

$$\boldsymbol{p}_e = \boldsymbol{p}_e(\theta), \qquad -\theta_{n_{mx}} \le \theta_n \le \theta_{n_{mx}}, \tag{1}$$

where $\theta_{n_{mx}}$ is the mechanical limit of the (n) joint.

Figure 1 shows the work area of the RE in the XY plane in the study with $\theta_{mx} = \pm 0.611\pi[rad]$. Here, a given set of joint combinations $A_{i\times 3} = [\theta_{i1} \quad \theta_{i2} \quad \theta_{i3}]$, where ($i$) is the number of combinations examined between the limits mentioned presented for 2 DoF, with three possible variants: $\theta_i^a = [0 \quad A_{i2} \quad A_{i3}]$, $\theta_i^b = [A_{i1} \quad 0 \quad A_{i3}]$, and $\theta_i^c = [A_{i1} \quad A_{i2} \quad 0]$. With 3 DoF, another two possible variants are $\theta_i^d = [A_{i1} \quad A_{i2} \quad A_{i2}]$ (used in [39]) and $\theta_i^e = [A_{i1} \quad A_{i2} \quad A_{i3}]$ (used in the test robot).

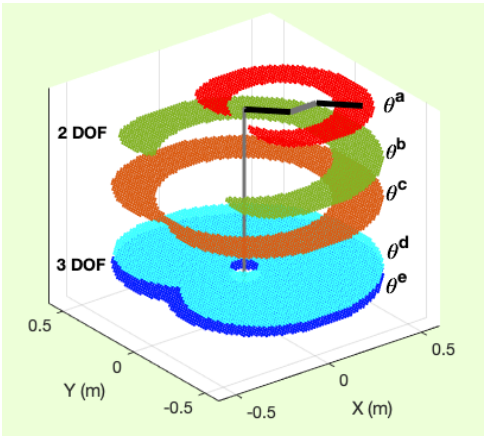

Fig. 1. Working areas for 2 DoF and 3 DoF configurations (Limit values for each joint: $\pm 0.61\pi[rad]$.

On the other hand, the final posture of the RE effector can be represented in a simple way, by the Operational Vector Space $\boldsymbol{x_e}$ ($m \times 1$), which is defined in the workspace according to the task to be performed by the manipulator, according to the expression (2) [40]

$$\boldsymbol{x}_e = [\boldsymbol{p}_e \quad \boldsymbol{\phi}_e]^T, \tag{2}$$

where $\boldsymbol{p}_e$ and $\boldsymbol{\phi}_e$ describe the final position and orientation of the effector, respectively; $(m \le n)$, where n is the number of joints of the robot. For the case of an RRR type planar robot, vector $\boldsymbol{x}_e$ is defined as $\boldsymbol{x_e} = [p_x \quad p_y \quad \phi]^T$, $(m = 3)$, where the coordinates p_x and p_y determine the position of the end effector, while ϕ is the orientation, in which $\phi = \theta_1 + \theta_2 + \theta_3$. Thereby, a manipulator is *inherently redundant* when the $\boldsymbol{x_e}$ dimension is less than the space dimension of the joints, where $(m < n)$. Moreover, in the case of $m = n$, a RE can be *functionally redundant* when $(r < m)$ is satisfied, where r is the number of $\boldsymbol{x_e}$ vector elements needed to specify a certain task. Finally, given the conditions of the task performed by the RE under study, it only considers the end position of the robot, excluding the orientation. So, this

structure offers a *functional redundancy* in the projected working conditions ($n = m = 3$, $r = 2$).

B. Polynomial Trajectory

A fourth degree polynomial trajectory (3) has five independent coefficients $(b_0 : b_4)$ and can satisfy the four constraints of a point-to-point trajectory, such as $\theta_n(0), \omega_n(0), \theta_n(f),$ and $\omega_n(f)$ - initial and final angular positions and angular speeds, respectively, for each joint (n). In this way, the fifth coefficient (b_4) is available as a control variable that allows the satisfaction of another restriction, which in this case will be used in the objective function for the optimization algorithm to represent the energy consumption of the manipulator

$$\theta_n(t) = b_0 + b_1\, t + b_2\, t^2 + b_3\, t^3 + b_4\, t^4, \tag{3}$$

where n is the joint number, $\theta_n(t)$ is the angular position of the joint n [rad], and b_j is the independent polynomial coefficients ($j = 0, \ldots, 4$).

Substituting the constraints of the problem into (3) through the polynomial independent coefficients, the expressions (4) to (7) are obtained as follows:

$$b_0 = \theta_{ni}, \tag{4}$$

$$b_1 = \dot{\theta}_{ni} = \omega_{ni}, \tag{5}$$

$$b_2 = \frac{[(3\theta_{nf} - 3\theta_{ni}) - (2\dot{\theta}_{ni} + \dot{\theta}_{nf})T + b_4 T^4]}{T^2}, \tag{6}$$

$$b_3 = \frac{[(2\theta_{ni} - 2\theta_{nf}) - (\dot{\theta}_{ni} + \dot{\theta}_{nf})T - 2b_4 T^4}{T^3}, \tag{7}$$

where T is the trajectory period [s], θ_{ni}, θ_{nf} are the initial and final angular positions in [rad], and $\dot{\theta}_{ni} = \omega_{ni}$ and $\dot{\theta}_{nf} = \omega_{nf}$ are the initial and final angular velocity [rad/s], respectively, for each n^{th} joint. Furthermore, b_2 and b_3 are in terms of the fifth coefficient b_4, which in the case of a 3 DoF manipulator correspond to a vector $\boldsymbol{b_4} = [b_{4_1} \quad b_{4_2} \quad b_{4_3}]$.

Subsequently, the value of the fifth coefficient (b_4) is obtained by means of an optimization algorithm that allows generating a trajectory of movements according to the initial constraints of the problem, in addition to satisfying the criteria of minimum energy consumption.

C. Objective Function

In the optimization problem described here, a variable related to the energy used by the robotic manipulator must be considered. In this case, for the objective function (OF) related to the energy consumption that represents this variable, it is proposed to experiment with three different approaches based on the torque derived from the calculation of the inverse dynamics of the manipulator under study.

These approaches are *total work* (J_W), *mean square torque* (J_τ), and *mechanical power* (J_p). Also, along with the OF tested, a weighting factor called "vector $\boldsymbol{K} = [k_1 \quad k_2 \quad k_3]$" or "OWV" is used to differentiate the influence of each joint in the total response of this indicator.

1. *Total work* (J_W)

Abe [13] uses the expression based on (8) in the OF to represent the operating energy of the manipulator and is related to the total work performed during a specific trajectory. It integrates the absolute torque value used by each joint with respect to the angular position of its movement

$$J_W = \sum_{i=1}^{n} k_i \int_{\theta_{0_i}}^{\theta_{f_i}} \left|\tau_i(\theta)\right| d\theta, \tag{8}$$

where (n) is the number of joints of the robotic manipulator, (τ_i) is the torque of the i^{th} joint, and $(\theta_{0_i}, \theta_{f_i})$ correspond to the initial and final angular positions of the i^{th} joint, respectively, in the trajectory studied. Additionally, in this work, a weighting factor (k_i) is applied and is related to OWV.

2. *Mean square torque* (J_τ)

Expression (9) is considered in the OF by Hansen, Öltjen, Meike, and Ortmaier [9], corresponding to the total mean square torque of the articular, which is defined as the sum of the mean square torques of the manipulator's joints at each point on the trajectory

$$J_\tau = \sum_{i=1}^{n} k_i \frac{1}{2} \int_{t_0}^{t_f} \left|\tau_i(t)\right|^2 dt, \tag{9}$$

where (n) is the number of joints of the robotic manipulator, (τ_i) is the torque of the i^{th} joint and (t_0, t_f) correspond to the initial and final time, respectively, of the trajectory under study. Additionally, in this work, a weighting factor (k_i) is applied and is related to OWV. Finally, there are other works that exist, such as in [3], [14], and [19], that use alternative ways to calculate the square torque results of each joint.

3. *Mechanical power* (J_p)

In [9], the use of the product between torque and angular velocity is also considered as an alternative to specify the energy consumption of robotic equipment, which corresponds to mechanical power, defined in (10)

$$J_p = \sum_{i=1}^{n} k_i \int_{t_0}^{t_f} \left|\tau_i(t) \times \omega_i(t)\right| dt, \tag{10}$$

where (n) is the number of joints of the robotic manipulator, (τ_i) is the torque of the i^{th} joint, $\omega_i(t)$ is the angular velocity of the i^{th} joint, and (t_0, t_f) correspond to the initial and final time, respectively, in the trajectory under study. Additionally, in this work, a weighting factor (k_i) is applied and is related to OWV.

D. Manipulator Kinematics

For the development of this work, a simplified model of the redundant SCARA-type 5 DoF robotic manipulator, PRRRP-type, made by Urrea-Kern in [39] is used. Thus, the present study considers only the rotational component of the RE seen in [39], obtaining a redundant system of 3 DoF in an XY plane, according to Fig. 2.

Therefore, only the rotational component of the RE seen in [39] is considered here, obtaining a redundant 3 DoF system in the XY plane. According to the kinematic scheme (Fig. 2(b)), the first prismatic articulation subscript must be subtracted to each subscript of the variables and parameters indicated in this diagram, with the aim of setting the parameters of this work according to the standard Denavit-Hartenberg method, shown in Table I.

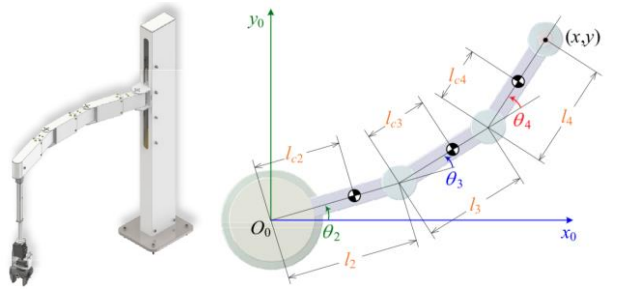

(a) (b)

Fig. 2. (a) Rotationally and prismatically redundant SCARA-type robot [39]; (b) Kinematic scheme of the redundant rotational component [39].

TABLE I. DENAVIT-HARTEBERG PARAMETERS.

$\boldsymbol{\theta_i}$	$\boldsymbol{\alpha}$	$\boldsymbol{r_i}$	$\boldsymbol{d_i}$
θ_1	0	l_1	0
θ_2	0	l_2	0
θ_3	0	l_3	0

In Table I, l_n and θ_n correspond to the length of the n_{th} link and the angle of the n_{th} joint, respectively, for n = {1, 2, 3}.

1. *Direct Kinematics*

The solution to the direct kinematics problem is obtained from the position vector [$\boldsymbol{p}$], beginning with the development of the homogeneous matrix for its three DoF, according to (11):

$$\begin{bmatrix} \boldsymbol{n} & \boldsymbol{o} & \boldsymbol{a} & \boldsymbol{p} \\ 0 & 0 & 0 & 1 \end{bmatrix} = \boldsymbol{T} = {}^0\boldsymbol{T}_1 \times {}^1\boldsymbol{T}_2 \times {}^2\boldsymbol{T}_3 = {}^0\boldsymbol{T}_3, \tag{11}$$

$${}^0T_3 = \begin{bmatrix} c_{123} & -s_{123} & 0 & l_1c_1 + l_2c_{12} + l_3c_{123} \\ s_{123} & c_{123} & 0 & l_1s_1 + l_2s_{12} + l_3s_{123} \\ 0 & 0 & 1 & 0 \\ 0 & 0 & 0 & 1 \end{bmatrix}, \tag{12}$$

where $c_1 = cos(\theta_1)$, $s_1 = sin(\theta_1)$, $c_{12} = cos(\theta_1 + \theta_2)$, $s_{12} = sin(\theta_1 + \theta_2)$, $c_{123} = cos(\theta_1 + \theta_2 + \theta_3)$ and $s_{123} = sin(\theta_1 + \theta_2 + \theta_3)$.

2. *Inverse Kinematics*

Considering the inverse kinetics problem for a 3 DoF planar manipulator, two different solution methods are presented:

Algebraic calculation method. First, the problem is simplified by considering $\phi = \theta_1 + \theta_2 + \theta_3$. Then, from the components T_{14} and T_{24} of the position vector [p] of the expression (12), the cosine θ_2 (13) is obtained. Then, by means of some trigonometric rules and simplifications, the other trigonometric functions (14)–(16) needed to determine the angles of the joints are obtained as a function of the coordinates (x, y) and the parameter ϕ:

$$c_2 = \frac{(x - l_3c_\phi)^2 + (y - l_3s_\phi)^2 - l_1^2 - l_2^2}{2l_1l_2}, \tag{13}$$

$$\theta_2 = \arctan\left(\frac{\pm s_2}{c_2}\right), \tag{14}$$

$$\theta_1 = \arctan\left(\frac{s_1}{c_1}\right), \tag{15}$$

$$\theta_3 = \phi - \theta_1 - \theta_2. \tag{16}$$

– Calculation method from homogeneous matrix. Initially, the problem is simplified [39] considering $\theta_2 = \theta_3$ and $l_1 = l_2 = l_3 = l$. Subsequently, from T_{14} and T_{24} of the expression (12), the angle θ_2 is determined according to (17)

$$\theta_2 = \pm\arccos\left(-\frac{1}{2} \pm \frac{\sqrt{x^2 + y^2}}{2l}\right). \tag{17}$$

Subsequently, from the equations developed from the homogeneous matrix (11) and suitably solving for ${}^2\boldsymbol{T}_3$, it is possible to determine θ_1, obtaining the expression (18)

$$\theta_1 = arctan\left(\frac{y}{x}\right) - \theta_2. \tag{18}$$

Finally, the inverse kinematic solution for a 2 DoF planar manipulator is obtained through geometric methods, according to the expressions (19) and (20):

$$\theta_1 = \beta \mp \alpha_k, \tag{19}$$

$$\theta_2 = \pm(\pi - \gamma), \tag{20}$$

where:

$$\alpha_k = \arccos\left(\frac{-l_2^2 + l_1^2 + \sqrt{x^2 + y^2}}{2l_1\sqrt{x^2 + y^2}}\right), \tag{21}$$

$$\beta = arctan\left(\frac{y}{x}\right), \tag{22}$$

$$\gamma = arccos\left(\frac{l_1^2 + l_2^2 - \sqrt{x^2 + y^2}}{2l_1l_2}\right). \tag{23}$$

At last, it should be noted that all expressions with double sign ($\pm$) imply the possibility of obtaining a second solution for the same RE configuration (the same extreme-end position in the workspace).

E. Manipulator Dynamics

The general Euler-Lagrange equation of motion for the dynamic model of a manipulator with n joints is defined in its matrix representation according to (24)

$$\boldsymbol{\tau} = \boldsymbol{D}(\theta)\ddot{\boldsymbol{\theta}}(t) + \boldsymbol{C}(\theta, \dot{\theta})\dot{\boldsymbol{\theta}}(t) + \boldsymbol{F}(\dot{\theta}) + \boldsymbol{g}(\theta), \tag{24}$$

where n is the number of manipulator joints, $\boldsymbol{\tau}$ is the (n × 1) generalized torque vector, $\dot{\boldsymbol{\theta}}(t)$ is the (n × 1) manipulator

arm joints' angular velocity vector, $\ddot{\boldsymbol{\theta}}(t)$ is the (n × 1) manipulator arm joints' acceleration vector, $\boldsymbol{D}(\theta)$ is the (n × n) symmetric inertia matrix, $\boldsymbol{C}(\dot{\theta})$ is the (n × n) Coriolis and centrifugal forces vector, $\boldsymbol{F}(\dot{\theta})$ is the (n × 1) friction vector, and $\boldsymbol{g}(\theta)$ is the (n × 1) gravitational load force vector.

The following assumptions and considerations have been made in the development of dynamic equations for the aforementioned robot manipulator:

– Dynamic equation calculation method: Euler-Lagrange (Asada-Spong);

– The manipulator's level is perfectly even to the system's base {0}, which allows considering a null influence of gravity in the system;

– All links' inertial products are considered null.

Friction. The dynamic effects due to the manipulator's transmission systems cause an increase in frictional forces, which are considered mechanical losses and should be taken into account when conducting an energy optimization study. This phenomenon is represented through different models according to Liu, Li, Zhang, Hu, and Zhang [41] and Prevez and Muman [42]. Thus, in Fig. 3, this behavior is shown with different degrees of precision where the viscous friction model (25), Coulomb and Viscous friction model (26), and the Stribeck friction model (27) are represented:

$$\tau_{fvi} = B_i\dot{\theta}_i, \tag{25}$$

$$\tau_{fcvi} = B_i\dot{\theta}_i + \tau_{ci}, \tag{26}$$

$$\tau_{fsti} = B_i\dot{\theta}_i + \left(\tau_{ci} + (\tau_{si} - \tau_{ci})e^{-\left|\frac{\dot{\theta}_i}{v_s}\right|^{\delta}}\right)sgn(\dot{\theta}_i), \tag{27}$$

where τ_{fvi} is the viscous friction model force of the i^{th} joint (25), τ_{fcvi} is the Coulomb-Viscous friction model force of the i^{th} joint (26), τ_{fsti} is the Stribeck friction model force of the i^{th} joint (27), B_i is the viscous friction of the i^{th} joint, τ_{ci} is the Coulomb friction of the i^{th} joint, τ_{si} is the Static friction of the i^{th} joint, v_s is the Stribeck speed, and δ is the empirical dimensionless parameter.

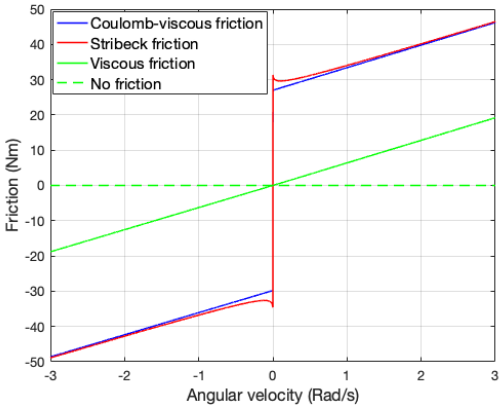

Fig. 3. Representative friction models versus speed characteristic.

Additionally, the behavior of the friction constants must be taken into account, which can take different values according to the direction of rotation of each joint, as stated in expression (25)

$$\tau_c = \begin{cases} 0: & si\ \dot{\theta} = 0, \\ \tau_c^+: & si\ \dot{\theta} > 0, \\ \tau_c^-: & si\ \dot{\theta} < 0, \end{cases} \quad \wedge \quad B = \begin{cases} 0: & si\ \dot{\theta} = 0, \\ B^+: & si\ \dot{\theta} > 0, \\ B^-: & si\ \dot{\theta} < 0. \end{cases} \tag{28}$$

Finally, the solutions for the matrices of (24) are shown through (29) to (44):

$$\begin{aligned} D_{11} &= l_1^2 m_1 + m_2(l_1^2 + l_{c2}^2 + 2l_1 l_{c2}c_2) + ... \\ &+ m_3(l_1^2 + l_2^2 + l_3^2 + 2l_1 l_{c3}c_{23} + 2l_2 l_{c3}c_3 + 2l_1 l_2 c_2) + ... \\ &+ I_{1zz} + I_{2zz} + I_{3zz}, \end{aligned} \tag{29}$$

$$\begin{aligned} D_{12} = D_{21} &= m_2(l_{c2}^2 + l_1 l_{c2}c_2) + ... \\ &m_3(l_2^2 + l_{c3}^2 + l_1 l_{c3}c_{23} + 2l_2 l_{c3}c_3 + l_1 l_2 c_2) + ... \\ &I_{2zz} + I_{3zz}, \end{aligned} \tag{30}$$

$$D_{13} = D_{31} = m_3(l_{c3}^2 + l_1 l_{c3}c_{23} + l_2 l_{c3}c_3) + I_{zz3}, \tag{31}$$

$$\begin{aligned} D_{22} &= m_2(l_{c2}^2) + m_3(l_{c3}^2 + 2l_2 l_{c3}c_3 + l_2^2) + ... \\ &+ I_{2zz} + I_{3zz}, \end{aligned} \tag{32}$$

$$D_{23} = D_{32} = m_3(l_{c3}^2 + l_2 l_{c3}c_3) + I_{zz3}, \tag{33}$$

$$D_{33} = m_3(l_{c3}^2) + I_{zz3}, \tag{34}$$

$$\begin{aligned} C_{11} &= -(l_{c2}m_2 + l_2 m_3)l_1 s_2 \dot{\theta}_2 - (l_2 l_{c3}m_3 s_3)\dot{\theta}_3 + ... \\ &-(l_1 l_{c3}m_3 s_{23})(\dot{\theta}_2 + \dot{\theta}_3), \end{aligned} \tag{35}$$

$$\begin{aligned} C_{21} &= (l_1 l_{c2}m_2 s_2 + l_1 l_{c3}m_3 s_{23} + l_1 l_2 m_3 s_2)\dot{\theta}_1 + ... \\ &-l_2 l_{c3}m_3 s_3 \dot{\theta}_3, \end{aligned} \tag{36}$$

$$C_{31} = l_1 l_{c3}m_3 s_{23}\dot{\theta}_1 - l_2 l_{c3}m_3 s_3(\dot{\theta}_1 + \dot{\theta}_2), \tag{37}$$

$$\begin{aligned} C_{12} &= -(l_{c2}m_2 + l_2 m_3)l_1 s_2(\dot{\theta}_1 + \dot{\theta}_2) + ... \\ &-l_2 l_{c3}m_3 s_3 \dot{\theta}_3 - (l_1 l_{c3}m_3 s_{23})(\dot{\theta}_1 + \dot{\theta}_2 + \dot{\theta}_3), \end{aligned} \tag{38}$$

$$C_{22} = -(l_2 l_{c3}m_3 s_3)\dot{\theta}_3, \tag{39}$$

$$C_{32} = (l_2 l_{c3}m_3 s_3)(\dot{\theta}_1 + \dot{\theta}_2), \tag{40}$$

$$\begin{aligned} C_{13} &= -(l_1 l_{c3}m_3 s_{23})(\dot{\theta}_2 + \dot{\theta}_3) + ... \\ &-l_2 l_{c3}m_3 s_3(\dot{\theta}_1 + \dot{\theta}_2 + \dot{\theta}_3), \end{aligned} \tag{41}$$

$$C_{23} = -(l_2 l_{c3}m_3 s_3)(\dot{\theta}_1 + \dot{\theta}_2 + \dot{\theta}_3), \tag{42}$$

$$C_{33} = 0, \tag{43}$$

$$\boldsymbol{F}(\dot{\theta}) = [\tau_{f1} \quad \tau_{f2} \quad \tau_{f3}]^T, \quad \boldsymbol{g}(\theta) = [0 \quad 0 \quad 0]^T, \tag{44}$$

where $S_2 = sin(\theta_2)$, $C_2 = cos(\theta_2)$, $S_3 = sin(\theta_3)$, $C_3 = cos(\theta_3)$, $S_{23} = sin(\theta_2 + \theta_3)$, $C_{23} = cos(\theta_2 + \theta_3)$, m_i is the mass of the i^{th} link [kg], l_{ci} is the length from the origin of the i^{th} link to its center of mass (centroid) [m], and τ_{fi} is a friction term of the i^{th} joint;

III. PROPOSED SOLUTION

A. Proposed Algorithm

According to Fig. 4, with the aim of solving the aforementioned problem, a nested optimization algorithm with two loops is proposed. The outer loop - belonging to optimization algorithm 1 - is responsible for obtaining both

the OWV $\boldsymbol{K}^* = [k_1^* \quad k_2^* \quad k_3^*]$ and the optimal vectors θ_i^*, θ_f^*, which correspond to the best initial and final angular positions given a certain trajectory. On the other hand, the inner loop - belonging to optimization algorithm 2 - takes care of determining the optimal vector $\boldsymbol{b}_4^* = [b_{4_1}^* \quad b_{4_2}^* \quad b_{4_3}^*]$, which corresponds to the fifth coefficient related to the fourth degree polynomial used to construct the desired trajectory. Here, in each iteration, the candidate values $\boldsymbol{K}^c, \boldsymbol{\theta}_i^c, \boldsymbol{\theta}_f^c$, and $\boldsymbol{b}_4^c$ are employed until the closest possible value to the minimum of the global cost function is found.

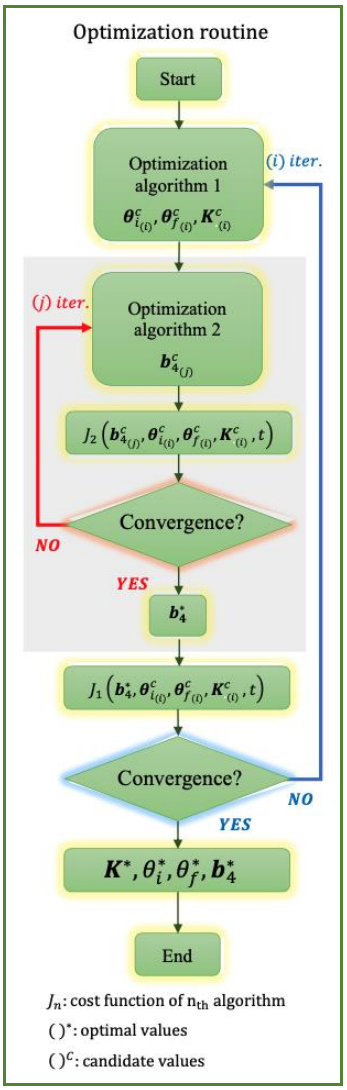

Fig. 4. Optimization routine of the double-loop algorithm under study.

B. Manipulator Parametrization

For the configuration of the generic manipulator model (24), the parameters related to the three rotational joints of the robot manipulator, studied by Urrea-Kern in [39], are used, where $l_{c1} = l_{c2} = l_{c3} = 0.0229\,[m]$, $l_1 = l_2 = l_3 = 0.2\,[m]$, $m_1 = m_2 = 1.023\,[kg]$, and $m_3 = 1.5344\,[kg]$. In the latter case, the mass of the fifth link in the model [39] is added to m_3; Furthermore, given that friction is a dominant dynamic characteristic in the study of the energy consumption of an RE and considering the information available on the friction specifications of the robot under study according to Table II, the friction model used here is Coulomb-Viscous (26).

TABLE II. FRICTION PARAMETERS OF THE ROTATIONAL JOINTS CONSIDERED FOR THE SCARA TYPE MANIPULATOR [39].

Parameter	Value	Unit
B_1	0.025	[*Nms/rad*]
τ_{c1}^-	-0.05	[*Nm*]
τ_{c1}^+	0.05	[*Nm*]
B_2	0.025	[*Nms/rad*]
τ_{c2}^-	-0.05	[*Nm*]
τ_{c2}^+	0.05	[*Nm*]
B_3	0.025	[*Nms/rad*]
τ_{c3}^-	-0.05	[*Nm*]
τ_{c3}^+	0.05	[*Nm*]

C. Test Trajectories

The RE workspace in the XY plane is conditioned to the maximum angle $\pm\theta_{mx}$ of each joint and its possible joint combinations. So, before defining the test trajectories, work surfaces are established for each operational variant to be tested with the manipulator. This is to trace the routes within such areas.

Figure 5 shows two working areas drawn by the manipulator under study. The first (plotted in cyan) comes from the direct kinematics calculation (12) of 68563 different sample combinations of the generalized coordinate vector $\boldsymbol{q}^e = [\theta_1 \quad \theta_2 \quad \theta_3]^T$, while the second (plotted in red) comes from the direct kinematics calculation (12) of 5768 combinations of the generalized coordinate vector $\boldsymbol{q}^d = [\theta_1 \quad \theta_2 \quad \theta_3]^T$, with the restriction $\theta_2 = \theta_3$. The latter condition explains the differences between these graphics. In both cases, the articular movement (θ_n) is limited to $-\theta_{mx} \le \theta_n \le \theta_{mx}$, where θ_{mx} = 110 ° is the maximum angle for each joint.

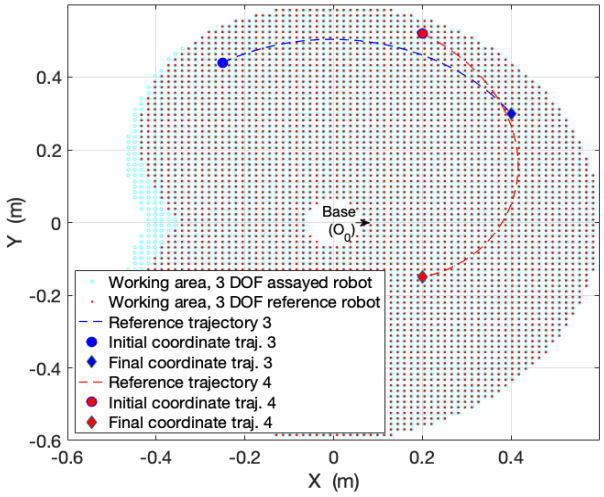

Fig. 5. Working areas of the robots and test trajectories 1 and 2.

In addition, Fig. 6 shows a comparison between the 3 DoF and 2 DoF variants of the manipulator under study. Here, the working area of the red dots comes from direct kinematics calculations (12) of 1770 different sample

combinations of the generalized coordinate vector $\boldsymbol{q}^a = [\theta_1 \quad \theta_2 \quad \theta_3]^T$, constrained by θ_1 = 0 (first joint blocked at 0 radians). In the 3 DoF version (plotted in cyan), the working area comes from q^e, as seen in the previous case. Similarly, for the case of the other 2 DoF tested variants considered, these will be locked to 0 radians at the second and third joint, respectively (θ_2 = 0 or θ_3 = 0).

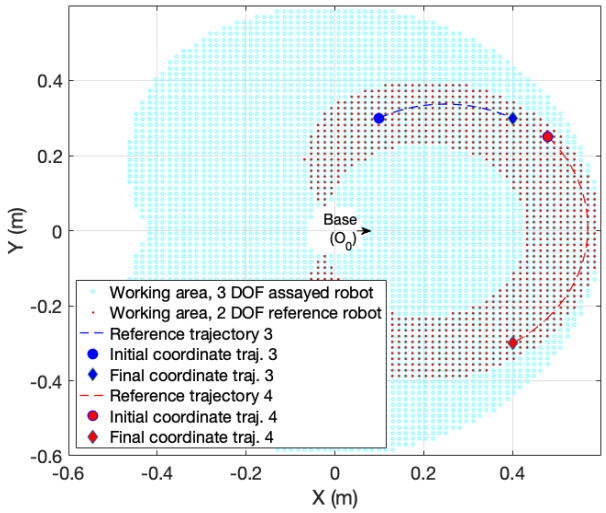

Fig. 6. Working areas of robots and test trajectories 3 and 4.

Four experiments were performed, with two test trajectories (TT) each. In every essay, the performance of the RE, running by the optimized trajectory obtained with the proposed test algorithm (Fig. 4), is compared to one of the four operation variants; this is detailed below.

The first experiment employs, as a comparison reference, an operational variant of the RE running with 3 DoF and a point-to-point trajectory based on third-order polynomials ($\boldsymbol{b_4}$ = 0), whose initial and final joint configurations are obtained from the homogeneous matrix method, where θ_2 = θ_3, as seen in [39]. The other three operation variants of comparison suppose the RE running with 2 DoF (locking a joint) in the XY plane; for this it is considered $\theta_1 = 0\,[rad], \theta_2 \wedge \theta_3 = \{-\theta_{mx}, ..., \theta_{mx}\}$ in the second experiment, $\theta_2 = 0\,[rad], \theta_1 \wedge \theta_3 = \{-\theta_{mx}, ..., \theta_{mx}\}$ in the third experiment, and $\theta_3 = 0\,[rad], \theta_1 \wedge \theta_2 = \{-\theta_{mx}, ..., \theta_{mx}\}$ in the fourth experiment. Furthermore, a point-to-point trajectory based on the third-order polynomials has been developed here, whose initial and final joint configurations are obtained from the geometric method mentioned above. It should be noted that in the tests with 2 DoF, certain masses of the links have been modified according to the locked joint.

Additionally, the eight test trajectories assayed are bounded by the following constraints: $\theta_{mx} = \pm 110\,° (\pm 1.9198\,[rad])$, travel time or trajectory period of t = 1.5 [*seg.*], initial and final speeds and accelerations $\dot{\theta}_i = \dot{\theta}_f = \ddot{\theta}_i = \ddot{\theta}_f = 0$. Table III shows the defined Cartesian coordinates for the start and end points of the eight tested trajectories. Figures 5 and 6 show the reference trajectories (inside the RE workspace) used in experiments 1 to 4, respectively.

TABLE III. INITIAL AND FINAL COORDINATES OF THE TEST TRAJECTORIES (TT) AND SIZE OF THE REGISTER OF JOINT COMBINATIONS (RJC).

TT	Initial Cartesian coordinate [x, y]	Final Cartesian coordinate [x, y]	Unit	Size RJC
1	[0.2, 0.52]	[0.2, -0.15]	[*m*]	50516
2	[-0.25, 0.44]	[0.4, 0.3]	[*m*]	21364
3	[0.1, 0.3]	[0.4, 0.3]	[*m*]	29064
4	[0.48, 0.25]	[0.4, -0.3]	[*m*]	88752
5	[-0.12, 0.5]	[0.3, 0.43]	[*m*]	50912
6	[0.36, 0.43]	[0.36, -0.35]	[*m*]	71136
7	[-0.12, 0.5]	[0.3, 0.43]	[*m*]	50912
8	[0.36, 0.43]	[0.36, -0.35]	[*m*]	71136

D. Optimization Algorithms

The implementation of the proposed algorithm in Fig. 4 requires the use of optimization variables of continuous and integer types, so this work becomes an optimization problem known as Mixed Integers. Continuous variables are the OWV and the $\boldsymbol{b_4}$ vector (fifth coefficient of the fourth-order polynomial). These can take any value between the boundary conditions defined by the vectors ***Lb*** and ***Ub*** (lower bound, upper bound), previously configured in each optimization algorithm. On the other hand, the integer optimization variable is related to the pointer values of the RJC, which stores the combinations previously determined for the initial and final joint positions (θ_i and θ_f) of the manipulator robot, given a determined point-to-point trajectory.

The RJC is constructed using the inverse kinematics calculation by means of the algebraic method described above. Initially, a series of (k) consecutive values is established as follows: $\phi_k = \{-3\theta_{mx_0}, ..., 3\theta_{mx_k}\}$, where $\phi = \theta_1 + \theta_2 + \theta_3$. With these values, in addition to the initial and final Cartesian coordinates of the path to be optimized, all the possible combinations of joints contained within the previously defined θ_{mx} constraints can be achieved using the just-named inverse kinematics calculation method. Thus, 1152 different values (equals to k) of initial and final joint configurations are obtained, according to the different test trajectories shown in Table III, where the size of the RJC is also shown.

The outer loop of the algorithm under study (Fig. 4) is tested with two different optimization routines, both capable of solving a mixed-integer problem; the first uses a Genetic Algorithm (GA), and the second uses a Surrogate Algorithm (SG).

The GA is a software optimization mechanism based on a natural selection process that mimics biological evolution. The algorithm repeatedly modifies a population of individual solutions. At each step, the GA randomly selects individuals from the current population and uses them as "parents" to produce "children" for the next generation. In this way, over successive generations, the population "evolves" towards an optimal solution. The most significant configuration parameters used here with MatLab's solver are shown in Table IV, where R_x corresponds to the last pointer in the RJC register associated with the trajectory under study.

The Surrogate Algorithm (SG) is a space-mapping type

optimization algorithm. This algorithm builds a *surrogate model* of the cost function by initially defining random points and interpolating them by means of a cubic-type radial basis function. The model is then evaluated within the original cost function. It implements a "merit function" based on hundreds of semi-randomly distributed sample points near the tested optimal point (possible optimal zone); then, the merit function chooses the best candidate from these samples and evaluates it within the objective function of the problem. This operation is done iteratively until the algorithm returns the best solution found during optimization. The SG algorithm is characterized by its rapid response thanks to the minimal evaluations it performs with the cost function, so it easily adapts to problems with functions that require high computational cost. Table V presents the most significant configuration parameters of the SG algorithm used here, with the MATLAB solver.

On the other hand, the inner loop of the algorithm under study (algorithm 2, Fig. 4) is implemented by means of the MATLAB nonlinear programming solver ("fmincon"), using the Interior Point optimization algorithm (IP). IP is an iterative algorithm that starts by identifying a feasible trial solution. In each iteration, it moves from a "current test solution" to a "better test solution" over the feasible region, until a solution that is essentially optimal is reached. In particular, the MATLAB solver follows a barrier approach that uses sequential quadratic programming and trusts regions to solve the subproblems that occur in the iteration. The most relevant configuration parameters used for Optimizer Algorithm 2 are shown in Table VI.

TABLE IV. CONFIGURATION PARAMETERS OF THE GA ALGORITHM USED.

GA Parameter	**Value**
PopulationSize:	50
CrossoverFraction:	0, 8
Lower bounds (Lb):	[0 0 0 1]
Upper bounds (Ub):	[20 5 5 R_x]
Intcon:	4
nvars:	4
PopulationSize:	50

TABLE V. CONFIGURATION PARAMETERS OF THE SG ALGORITHM USED.

SG Parameter	**Value**
Max. function evaluations	200
Min. surrogate points	20
Lower bounds (Lb):	[0 0 0 1]
Upper bounds (Ub):	[20 5 5 R_x]
Min. sample distance	1×10^{-3}
nvars:	4
Intcon:	4

TABLE VI. CONFIGURATION PARAMETERS OF THE ALGORITHM PI USED.

Parameter IP	**Value**
Algorithm:	"interior-point"
MaxIterations:	1000
Lower bounds (Lb):	[-.1 -.1 -.1]
Upper bounds (Ub):	[.1 .1 .1]
Initial condition (K0):	[0 0 0]

To assess the performance of the proposed algorithm, the results will be determined by the percentage difference between the torques resulting from the reference trajectory test and those from the optimized trajectory test. In this case, a positive value of this difference represents an energy savings with respect to the reference trajectory. The torques derived from each trajectory are determined through the sum of the values of the root mean square (RMS) derived from the torques obtained from each joint, both for the case of the reference trajectory (τ^{ref}) and for the optimized trajectory (τ^{*}), according to the expressions declared in (45) and (46):

$$\tau^{ref} = \sum_{i=1}^{n} \sqrt{\frac{1}{T}\int_{t_0}^{t_f} \left|\tau_i^{ref}(t)\right|^2 dt}, \tag{45}$$

$$\tau^{*} = \sum_{i=1}^{n} \sqrt{\frac{1}{T}\int_{t_0}^{t_f} \left|\tau_i^{*}(t)\right|^2 dt}, \tag{46}$$

where n is the number of joints of the robotic manipulator, τ_i is the torque of the i^{th} joint, and (t_0, t_f) correspond to the initial and final time, respectively, in the trajectory studied.

IV. RESULTS

The results of the behavior of the proposed optimization algorithm are obtained from the software implementation of a 3 DoF planar robotic manipulator derived from the rotational component of a redundant SCARA-type robot, developed and implemented in [39]. The characteristic parameters of the RE are obtained from the same aforementioned work. The experiments were carried out on a computer with an Intel Core i5 CPU, clocked at 2 GHz, with 8 GB of RAM, running MatLab 2019b simulation software.

The following tables summarize the results for test trajectories 1 through 8. The experimental values obtained with two different optimization techniques in the main loop (GA and SG) are shown; three objective functions related to energy consumption have also been tested. The results correspond to the energy efficiency achieved with respect to the reference trajectory (third degree polynomial in different variants) and to the calculation time of the algorithm required to obtain the optimal trajectory.

Table VII shows the results of the test trajectories 1 and 2, compared with the reference trajectory obtained from the same 3 DoF robot under the previously established $\theta_2 = \theta_3$ condition. The results are presented with the three objective functions tested, where O.F. 1 is the mean square torque ($\boldsymbol{J_\tau}$), O.F. 2 is the total work ($\boldsymbol{J_W}$), and O.F. 3 is the mechanical power ($\boldsymbol{J_P}$). Furthermore, GA and SG correspond to the two algorithms tested in the outer loop. EF. is the efficiency [%], and T.C. is the total time calculation [s] of the proposed algorithm.

Tables VIII, IX, and X show the results of the test trajectories 3 to 8 compared to the reference ones obtained from the test robot operating with 2 DoF. In all three variants, $\boldsymbol{\theta_1 = 0}$ **[*rad*]**, $\boldsymbol{\theta_2 = 0}$ **[*rad*]**, and $\boldsymbol{\theta_3 = 0}$ **[*rad*]**, respectively. The results are presented with the three tested OFs, where O.F. 1 is the mean square torque ($\boldsymbol{J_\tau}$), O.F. 2 is the total work ($\boldsymbol{J_W}$), and O.F. 3 is the mechanical power ($\boldsymbol{J_P}$).

Furthermore, GA and SG correspond to the two algorithms tested in the outer loop. EF. is the efficiency [%] and T.C. is the total time calculation [s] of the proposed algorithm.

Likewise, Figs. 7 and 8 show the angular positions, the torques of the joints obtained, and the paths developed in the Cartesian plane for the test trajectories 2 and 6. All figures show the results of the polynomial optimized with respect to those of the reference path.

TABLE VII. RESULTS OF TEST TRAJECTORIES 1 AND 2.

		O.F. 1 (J_τ)		O.F. 2 (J_W)		O.F. 3 (J_P)	
Traject./Opt. Alg.	**τ_{ref} [Nm]**	**EF. [%]**	**T.C. [s]**	**EF. [%]**	**T.C. [s]**	**EF. [%]**	**T.C. [s]**
Traj. 1/GA	8.9	10.0	103.9	10.3	154.0	9.9	160.9
Traj. 1/SG	8.9	6.0	39.1	4.6	41.1	6.6	49.9
Traj. 2/GA	12.6	35.0	151.8	35.0	180.8	35.0	155.4
Traj. 2/SG	12.6	34.4	42.4	33.0	46.4	34.8	48.3

TABLE VIII. RESULTS OF TEST TRAJECTORIES 3 AND 4.

		O.F. 1 (J_τ)		O.F. 2 (J_W)		O.F. 3 (J_P)	
Traject./Opt. Alg.	**τ_{ref} [Nm]**	**EF. [%]**	**T.C. [s]**	**EF. [%]**	**T.C. [s]**	**EF. [%]**	**T.C. [s]**
Traj. 3/GA	4.5	27.0	141.3	26.8	146.8	26.8	137.1
Traj. 3/SG	4.5	26.8	38.1	24.9	40.9	25.8	52.0
Traj. 4/GA	8.2	31.3	128.3	30.9	157.8	31.3	199.7
Traj. 4/SG	8.2	30.1	40.5	30.2	45.9	29.7	44.5

TABLE IX. RESULTS OF TEST TRAJECTORIES 5 AND 6.

		O.F. 1 (J_τ)		O.F. 2 (J_W)		O.F. 3 (J_P)	
Traject./Opt. Alg.	**τ_{ref} [Nm]**	**EF. [%]**	**T.C. [s]**	**EF. [%]**	**T.C. [s]**	**EF. [%]**	**T.C. [s]**
Traj. 5/GA	5.4	17.8	118.2	19.3	146.1	17.5	206.2
Traj. 5/SG	5.4	18.3	40.3	18.0	41.6	19.2	49.8
Traj. 6/GA	9.9	9.5	103.7	10.0	146.7	9.8	167.5
Traj. 6/SG	9.9	9.5	32.1	9.9	38.5	9.7	43.7

TABLE X. RESULTS OF TEST TRAJECTORIES 7 AND 8.

		O.F. 1 (J_τ)		O.F. 2 (J_W)		O.F. 3 (J_P)	
Traject./Opt. Alg.	**τ_{ref} [Nm]**	**EF. [%]**	**T.C. [s]**	**EF. [%]**	**T.C. [s]**	**EF. [%]**	**T.C. [s]**
Traj. 7/GA	5.2	15.0	118.2	16.5	146.1	14.7	206.2
Traj. 7/SG	5.2	15.8	36.6	15.7	36.1	15.4	43.4
Traj. 8/GA	9.9	9.6	103.7	10.1	146.7	9.9	167.5
Traj. 8/SG	9.9	9.6	33.9	9.0	40.8	9.8	43.7

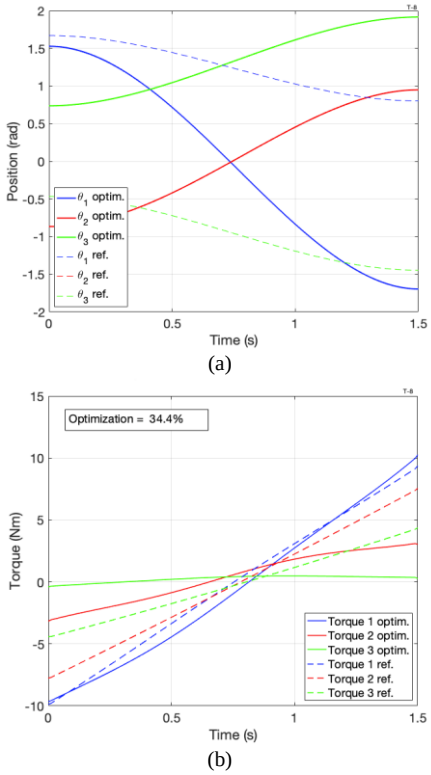

Fig. 7. Results of the test trajectory 2, applying polynomials optimized with the SG algorithm and OF: J_τ: (a) joint trajectories and (b) joint torques.

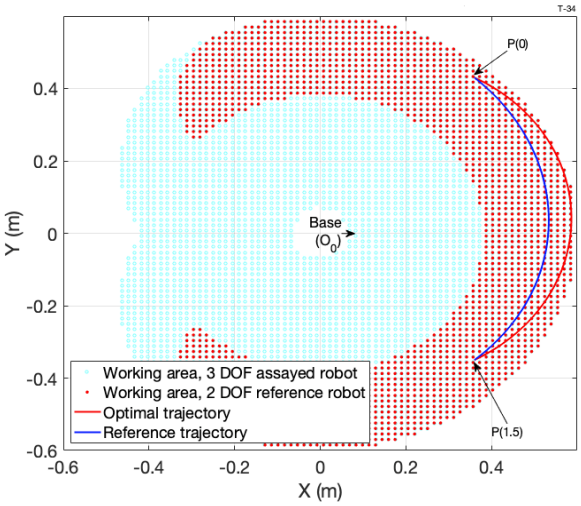

Fig. 8. Workspaces and paths developed in the XY Cartesian plane for the test trajectory 6, applying polynomials optimized with the SG algorithm and OF: J_W.

V. DISCUSSION

According to the experiments carried out, it can be seen (from Tables VII to X) that both algorithms tested (GA and SG) showed important energy savings with respect to the reference trajectory. The GA algorithm presented a slight improvement of 4.7 % over SG in the obtained energy

efficiency, while the SG algorithm exhibited a 72 % saving computational time over the GA algorithm. On the other hand, from the three objective functions related to energy consumption tested, the mean square torque has shown a significant saved computational time with 22 % with respect to total work and 40 % with respect to mechanical work.

To better favor the comparative analysis of the carried out tests, a *scatter diagram* is used, which allows one to develop a qualitative test study by inspecting the best combination of test factors. Likewise, a performance index is developed that allows quantitative determination of the better efficiency response versus calculation time. Therefore, according to the results obtained from the previous experiments, 48 samples were acquired, 6 for each test trajectory (TT). Figure 9 shows all the possible combinations between the optimization algorithms for the main loop (GA or SG) and the OFs considered for the tests. As a consequence of each of these combinations, a result or sample is obtained that represents the energy efficiency achieved (η) together with the calculation time (κ) to obtain the optimal trajectory sought.

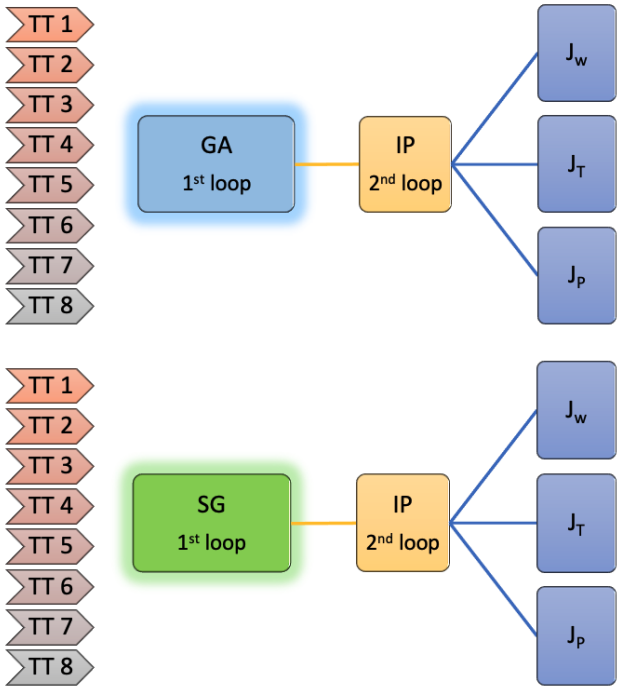

Fig. 9. Different experimental combinations.

A. Result Calculation Time Performance Index

To determine the best response of the proposed algorithm, considering the energy efficiency achieved and the greater economy of the calculation - given the different experiments carried out - a numeric performance indicator called the "Result Calculation Time Index" (RCTI) was developed (47). It considers the magnitude of the energy efficiency obtained (η) of a given sample. Then it is weighted between the range (1, 0] according to the absolute value of the sine of the angle α. This angle (48) is defined by the vector formed by the origin and a certain sample according to Fig. 10. In this way, it is sought to determine numerically the best performance response between energy efficiency and the calculation time of the optimization algorithm, favoring the minimum calculation time:

$$\mathrm{H} = \eta \left| \sin\alpha \right|, \tag{47}$$

$$\tan\alpha = \frac{\|\eta\|}{\|\kappa\|} = \frac{\eta / \max(\eta)}{\kappa / \max(\kappa)}, \tag{48}$$

where η is the efficiency [%] of the optimization algorithm in a given test, κ is the calculation time [s] of the optimization algorithm in the same test, and α is the angle defined by the vector formed by the origin and a certain sample.

B. Qualitative and Quantitative Analysis

Figure 10 presents 48 samples corresponding to the tests of the proposed algorithm. These are grouped by colors (24 samples for each solver instance), according to the two optimization algorithms tested in the main loop, and by shape (16 samples for each OF), according to the three OFs tested.

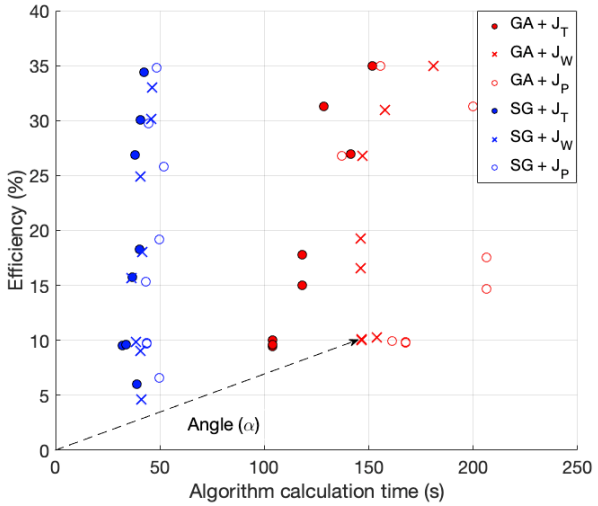

Fig. 10. (By shape) Comparison of the 3 different objective functions FO. (By colour) 2 variants of main loop optimization algorithms.

In all cases, the SG algorithm (plotted in blue) achieves a greater calculation economy compared to the GA (plotted in red). Likewise, the GA shows higher energy efficiency results compared to SG in all tests. However, this advantage is diminished by the calculation time of its response (> 50 seconds compared to SG). In addition, for the three OFs tested, the SG presents a lesser dispersion in the calculation time compared to the GA algorithm. In relation to OF performance, it is observed that in both cases (SG and GA), the mean square torque function (J_τ) showed better calculation times compared to its alternatives. Finally, all tests showed positive results in terms of energy efficiency. This establishes that the optimization algorithm proposed here, within all its variants, performs perfectly under the proposed test conditions.

On the other hand, by performing a quantitative analysis of the results obtained, using the performance index (RTCI), the graphs in Fig. 11 are obtained. In this case, the upper graph shows that the best combination corresponds to the mean square torque objective function (J_τ) combined with the surrogate optimization algorithm (SG). These results are consistent with the qualitative analysis previously carried out using the scatter plot. Likewise, according to the result

tables, a difference in the behavior of the energy consumption of the RE is observed between the tests with longitudinal and transverse trajectories with respect to the x-axis of the work plane. Although longitudinal trajectories require less energy during their execution, the possibility of energy optimization decreases, as seen in Fig. 11(b). In this case, the performance of the SG algorithm continues to stand out above that of the GA.

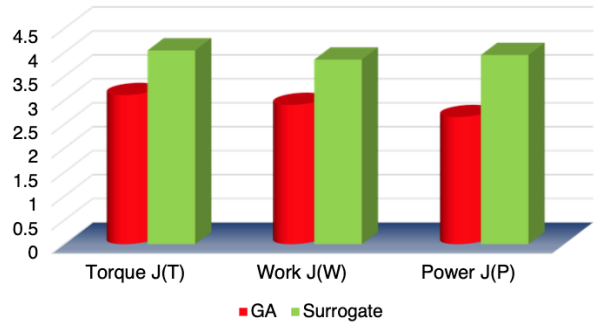

(a)

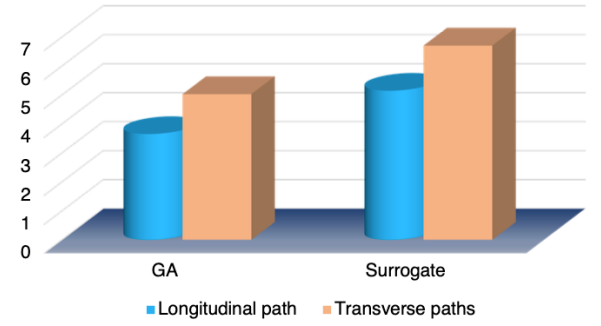

(b)

Fig. 11. (a) Performance (RTCI) of the two main loop algorithms, examined for the three different types of objective function FO; (b) Performance (RTCI) of the two main loop algorithms examined for longitudinal and transverse paths.

VI. CONCLUSIONS

According to the set of simulated done on the rotational component of a redundant SCARA type robot, which is parameterized the same as that of the robot used by Urrea-Kern in [39], it is desired to achieve energy savings in the execution of a planned point-to-point trajectory with the minimum calculation time, all in accordance with the test conditions presented here. Thus, it is sought to determine the best combination of test factors, as well as the objective functions and optimization algorithms, together with the optimal initial and final joint positions for each test.

The trajectory optimization process is based on fourth degree polynomials and focuses on the development of a nested two-loop optimization algorithm, where the outer loop determines, on the one hand, the Optimal Weighting Vector (OWV) which establishes the influence of each joint on the total energy consumption of the RE during the execution of a certain trajectory, and, on the other hand, the optimal combination of joint positions (initial and final) contained in the Register of Joint Combinations (RJC). The inner loop calculates the energetically optimal trajectory, considering both the dynamics of the robot and the optimal values of the OWV and the RJC.

In relation to the experiments, first, two point-to-point test trajectories were tested, which are compared between the 3 DoF test robots, and one with similar characteristics, but with different kinematic behavior (condition $\theta_2 = \theta_3$); here, three types of OF (related to the energy consumption of the robot) and two optimization algorithms were tested, which yields 12 experimental results in this test. The rest of the experiments compare the performance of the test robot with three variants of the robotic equipment operating with only 2 DoF. Each of these variants disables a certain joint by setting it to zero radians, leaving the other two joints operating within limits defined in the task, thus using the same configuration scenarios of the 3 DoF experiment; 36 results are obtained for each of the 6 test trajectories.

Given the number of results or samples derived from the tests (48 in total), a scatter diagram is used, which eases the elaboration of a qualitative study of the best combination of test factors. Likewise, a numerical performance indicator called the "Result Calculation Time Index" (RCTI) was developed, which allows quantitative determination of the best response between an energy efficiency route and the calculation time required to obtain it.

From the qualitative analyzes made, the following can be noticed. In relation to the optimization techniques tested in the main loop of the proposed algorithm, the Surrogate method stands out in the economy of calculation for all tests compared to the Genetic Algorithm. In addition, with respect to the three OFs tested, the same optimization algorithm presents less dispersion in calculation time with respect to the GA alternative. However, the GA optimization technique presents better results in the energy efficiency achieved for the planned trajectories. This is related to the better capacity of the algorithm to obtain a global minimum. This advantage is diminished by the calculation time in its response, which exceeds 50 [s] the Surrogate alternative's calculation time. In the case of the OFs tested, considering all test trajectories, the mean square torque (J_τ) stands out above the other two in terms of achieving an optimal highlight in the shortest possible computation time, indicating that this technique facilitates the work of optimization algorithms thanks to its way of computing the responses of the torques. Finally, it is observed that, in all the tests, the energy efficiency values obtained are greater than zero. This indicates that the optimization algorithm proposed here, with all its variants, has a positive performance under the proposed test conditions.

On the other hand, by performing a quantitative analysis of the results using the performance indicator (RTCI), it is established that the best combination for the simulated test trajectories corresponds to the mean square torque objective function (J_τ) combined with the algorithm Surrogate optimization (SG). Similarly, a difference in the behavior of the energy consumption of the robotic equipment is observed between the tests with longitudinal and transverse trajectories with respect to the x-axis of the working area. Although longitudinal paths certainly demand less energy during execution, the possibility of energy optimization decreases. In this case, the performance of the SG algorithm continues to stand out above that of the GA.

In summary, according to the observations of the

qualitative and quantitative analysis and in accordance with the test conditions presented here, the results allow inferring that the Surrogate optimization algorithm combined with a mean square torque cost function offers superior performance, with respect to the other combinations studied in this work. On the other hand, according to the tests carried out, the achieved energy savings are verified by adding a degree of redundancy to a task developed in the XY plane by a 2 DoF robotic equipment. This is due to the availability of a greater combination of joints that could contribute to more efficient alternative trajectories, from an energetic point of view.

CONFLICTS OF INTEREST

The authors declare that they have no conflicts of interest.

REFERENCES

[1] G. Carabin, E. Wehrle, and R. Vidoni, "A review on energy-saving optimization methods for robotic and automatic systems", *Robotics*, vol. 6, no. 4, p. 39, 2017. DOI: 10.3390/robotics6040039.

[2] S. Liu, Y. Wang, X. V. Wang, and L. Wang, "Energy-efficient trajectory planning for an industrial robot using a multi-objective optimisation approach", *Procedia Manuf.*, vol. 25, pp. 517–525, 2018. DOI: 10.1016/j.promfg.2018.06.122.

[3] Y. Liu, L. Liang, H. Han, and S. Zhang, "A method of energy-optimal trajectory planning for palletizing robot", *Math. Probl. Eng.*, vol. 2017, 2017. DOI: 10.1155/2017/5862457.

[4] P. Tokekar, N. Karnad, and V. Isler, "Energy-optimal trajectory planning for car-like robots", Department of Computer Science and Engineering University of Minnesota, Minneapolis, USA, Technical Rep. TR13-013, 2013.

[5] O. Wigstrom, B. Lennartson, A. Vergnano, and C. Breitholtz, "High-level scheduling of energy optimal trajectories", *IEEE Trans. Autom. Sci. Eng.*, vol. 10, no. 1, pp. 57–64, 2013. DOI: 10.1109/TASE.2012.2198816.

[6] P. Cezner, "Robotic trajectory optimization", Bachelor Project, Czech Technical University in Prague, Faculty of Electrical Engineering, Department of Control Engineering, 2017.

[7] S. Yin, W. Ji, and L. Wang, "A machine learning based energy efficient trajectory planning approach for industrial robots", *Procedia CIRP*, vol. 81, pp. 429–434, 2019. DOI: 10.1016/j.procir.2019.03.074.

[8] S. D. Das, V. Bain, and P. Rakshit, "Energy optimized robot arm path planning using differential evolution in dynamic environment", in *Proc. of 2018 Second International Conference on Intelligent Computing and Control Systems (ICICCS)*, 2018, pp. 1267–1272. DOI: 10.1109/ICCONS.2018.8663106.

[9] C. Hansen, J. Öltjen, D. Meike, and T. Ortmaier, "Enhanced approach for energy-efficient trajectory generation of industrial robots", in *Proc. of 2012 IEEE International Conference on Automation Science and Engineering (CASE)*, 2012, pp. 1–7. DOI: 10.1109/CoASE.2012.6386343.

[10] S. Pellegrinelli, S. Borgia, N. Pedrocchi, E. Villagrossi, G. Bianchi, and L. M. Tosatti, "Minimization of the energy consumption in motion planning for single-robot tasks", *Procedia CIRP*, vol. 29, pp. 354–359, 2015. DOI: 10.1016/j.procir.2015.02.174.

[11] J. C. Ramirez Henao and L. Duque Muñoz, "Optimización de manipulabilidad y consumo eléctrico mediante el Algoritmo Heurístico de Kalman en manipuladores seriales", *Ing. y Cienc.*, vol. 11, no. 21, pp. 51–71, 2015. DOI: 10.17230/ingciencia.11.21.3.

[12] C. Manríquez and D. H. O. Mendoza, "Generación de trayectorias en un manipulador serial de seis grados de libertad para reducir el consumo de energía", *Congr. Int. Investig.*, vol. 5, no. 3, 2013.

[13] A. Abe, "An effective trajectory planning method for simultaneously suppressing residual vibration and energy consumption of flexible structures", *Case Stud. Mech. Syst. Signal Process.*, vol. 4, pp. 19–27, 2016. DOI: 10.1016/j.csmssp.2016.08.001.

[14] K. K. Ayten, M. N. Sahinkaya, and A. Dumlu, "Optimum trajectory generation for redundant/hyper-redundant manipulators", *IFAC-PapersOnLine*, vol. 49, no. 21, pp. 493–500, 2016. DOI: 10.1016/j.ifacol.2016.10.651.

[15] P. Boscariol, G. Carabin, A. Gasparetto, N. Lever, and R. Vidoni, "Energy-efficient point-to-point trajectory generation for industrial robotic machines", in *Proc. of ECCOMAS Thematic Conference on Multibody Dynamics*, 2015.

[16] Y. Wang, Y. Zhao, S. A. Bortoff, and K. Ueda, "A real-time energy-optimal trajectory generation method for a servomotor system", *IEEE Trans. Ind. Electron.*, vol. 62, no. 2, pp. 1175–1188, 2015. DOI: 10.1109/TIE.2014.2360077.

[17] T. He, Y. Zhang, F. Sun, and X. Shi, "Immune optimization based multi-objective six-DOF trajectory planning for industrial robot manipulators", in *Proc. of 2016 12th World Congress on Intelligent Control and Automation (WCICA)*, 2016, pp. 2945–2950. DOI: 10.1109/WCICA.2016.7578610.

[18] X. Wang, X. Song, and W. Sun, "Surrogate based trajectory planning method for an unmanned electric shovel", *Mech. Mach. Theory*, vol. 158, art. 104230, 2021. DOI: 10.1016/j.mechmachtheory.2020.104230.

[19] S. Baressi Šegota, N. Anđelić, I. Lorencin, M. Saga, and Z. Car, "Path planning optimization of six-degree-of-freedom robotic manipulators using evolutionary algorithms", *Int. J. Adv. Robot. Syst.*, vol. 17, no. 2, pp. 1–16, 2020. DOI: 10.1177/1729881420908076.

[20] S. Liu, Y. Wang, X. V. Wang, and L. Wang, "Energy-efficient trajectory planning for an industrial robot using a multi-objective optimisation approach", *Procedia Manuf.*, vol. 25, pp. 517–525, 2018. DOI: 10.1016/j.promfg.2018.06.122.

[21] B. J. Martin and J. E. Bobrow, "Minimum-effort motions for open-chain manipulators with task-dependent end-effector constraints", *Int. J. Rob. Res.*, vol. 18, no. 2, pp. 213–224, 1999. DOI: 10.1177/02783649922066169.

[22] Y. Zhao, H.-C. Lin, and M. Tomizuka, "Efficient trajectory optimization for robot motion planning", in *Proc. of 2018 15th Int. Conf. Control. Autom. Robot. Vision (ICARCV)*, 2018, pp. 260–265. DOI: 10.1109/ICARCV.2018.8581059.

[23] S. G. Ruiz, L. V. Calderita, A. Hidalgo-Paniagua, and J. P. Bandera Rubio, "Measuring smoothness as a factor for efficient and socially accepted robot motion", *Sensors*, vol. 20, no. 23, p. 6822, 2020. DOI: 10.3390/s20236822.

[24] X. Yu, M. Dong, and W. Yin, "Time-optimal trajectory planning of manipulator with simultaneously searching the optimal path", *Comput. Commun.*, vol. 181, pp. 446–453, Jan. 2022. DOI: 10.1016/j.comcom.2021.10.005.

[25] Y. Wen and P. R. Pagilla, "Path-constrained optimal trajectory planning for robot manipulators with obstacle avoidance", in *Proc. of 2021 IEEE/RSJ International Conference on Intelligent Robots and Systems (IROS)*, 2021, pp. 1421–1426. DOI: 10.1109/IROS51168.2021.9636674.

[26] T. Zhang, M. Zhang, and Y. Zou, "Time-optimal and smooth trajectory planning for robot manipulators", *Int. J. Control. Autom. Syst.*, vol. 19, no. 1, pp. 521–531, 2021. DOI: 10.1007/s12555-019-0703-3.

[27] A. Vysocký *et al.*, "Reduction in robotic arm energy consumption by particle swarm optimization", *Applied Sciences*, vol. 10, no. 22, p. 8241, 2020. DOI: 10.3390/app10228241.

[28] F. Yuan, D. Chen, C. Pan, J. Du, X. Wei, and M. Wang, "Application of optimal-jerk trajectory planning in gait-balance training robot", *Chinese J. Mech. Eng.*, vol. 35, art. no. 2, 2022. DOI: 10.1186/s10033-021-00665-1.

[29] Y. Liu *et al.*, "Evolutionary multi-objective trajectory optimization for a redundant robot in Cartesian space considering obstacle avoidance", *Mech. Sci.*, vol. 13, no. 1, pp. 41–53, 2022. DOI: 10.5194/ms-13-41-2022.

[30] X. Liu, C. Qiu, Q. Zeng, A. Li, and N. Xie, "Time-energy optimal trajectory planning for collaborative welding robot with multiple manipulators", *Procedia Manufacturing*, vol. 43, pp. 527–534, 2020. DOI: 10.1016/j.promfg.2020.02.174.

[31] F. Stuhlenmiller, D. Clever, S. Rinderknecht, M. Lutter, and J. Peters, "Trajectory optimization of energy consumption and expected service life of a robotic system", in *Proc. of 2021 IEEE/ASME International Conference on Advanced Intelligent Mechatronics (AIM)*, 2021, pp. 842–847. DOI: 10.1109/AIM46487.2021.9517539.

[32] X. Cao *et al.*, "A multi-objective particle swarm optimization for trajectory planning of fruit picking manipulator", *Agronomy*, vol. 11, no. 11, Nov. 2021. DOI: 10.3390/agronomy11112286.

[33] H. Wang, Q. Zhao, H. Li, and R. Zhao, "Polynomial-based smooth trajectory planning for fruit-picking robot manipulator", *Inf. Process.*

Agric., in press. DOI: 10.1016/j.inpa.2021.08.001.
[34] A. Tringali and S. Cocuzza, "Finite-horizon kinetic energy optimization of a redundant space manipulator", *Appl. Sci.*, vol. 11, no. 5, p. 2346, 2021. DOI: 10.3390/app11052346.
[35] P. Freeman, "Minimum jerk trajectory planning for trajectory constrained redundant robots", Ph.D. dissertation, Washington University in St. Louis, School of Engineering and Applied Science, Department of Electrical and Systems Engineering, 2012, pp. 5–24.
[36] P. Boscariol and D. Richiedei, "Trajectory design for energy savings in redundant robotic cells", *Robotics*, vol. 8, no. 1, p. 15, 2019. DOI: 10.3390/robotics8010015.
[37] V. V. M. J. S. Chembuly and H. K. Voruganti, "Trajectory planning of redundant manipulators moving along constrained path and avoiding obstacles", *Procedia Computer Science*, vol. 133, pp. 627–634, 2018. DOI: 10.1016/j.procs.2018.07.094.
[38] J. Nurmi and J. Mattila, "Global energy-optimal redundancy resolution of hydraulic manipulators: Experimental results for a forestry manipulator", *Energies*, vol. 10, no. 5, p. 647, 2017. DOI: 10.3390/en10050647.
[39] C. Urrea and J. Kern, "Modeling, simulation and control of a redundant SCARA-type manipulator robot", *Int. J. Adv. Robot. Syst.*, vol. 9, no. 2, 2012. DOI: 10.5772/51701.
[40] B. Siciliano, L. Sciavicco, L. Villani, and G. Oriolo, *Robotics: Modelling, Planning and Control*. Springer, 2009. DOI: 10.1007/978-1-84628-642-1.
[41] Y. F. Liu, J. Li, Z. M. Zhang, X. H. Hu, and W. J. Zhang, "Experimental comparison of five friction models on the same test-bed of the micro stick-slip motion system", *Mech. Sci.*, vol. 6, no. 1, pp. 15–28, 2015. DOI: 10.5194/ms-6-15-2015.
[42] H. B. Prevez and F. C. Muman, "Una actualización sobre la fricción, su compensación y métodos de control en sistemas electromecánicos", 2019.